



Cite this: *RSC Adv.*, 2020, 10, 29306

Received 9th June 2020
Accepted 23rd July 2020

DOI: 10.1039/d0ra05092j

rsc.li/rsc-advances

Predicting reactivity for bioorthogonal cycloadditions involving nitrones[†]

Masaya Nakajima,^a Didier A. Bilodeau^b and John Paul Pezacki^b

Nitrones are useful dipoles in both synthesis and in bioorthogonal transformations to report on biological phenomena. In bioorthogonal reactions, nitrones are both small and relatively easy to incorporate into biomolecules, while providing versatility in their ability to harbor different substituents that tune their reactivity. Herein, we examine the reactivities of some common and useful nitrone cycloadditions using density functional theory (DFT) and the distortion/interaction (D/I) model. The data show that relative reactivities can be predicted using these approaches, and useful insights gained further enhancing reactivities of both nitrones and their dipolarophile reaction partners. We find that D/I is a useful guide to understanding and predicting reactivities of cycloadditions involving nitrones.

Bioorthogonal chemistry provides important methods for creating covalent chemical linkages to enable the study of biological processes inside cells that are otherwise difficult to examine.^{1–6} A number of bioorthogonal reactions have been developed and are now used as techniques to efficiently, selectively and covalently link two reactive groups.^{7–14} In addition to bioorthogonality, the ability to react with high specificity within biological environments, as well as fast reaction kinetics are highly sought after, as they allow for the utility of chemistry at low concentrations needed for *in vivo* applications. Reactions involving nitrone dipoles are amongst the fastest bioorthogonal chemical reactions. These include strain-promoted alkyne-nitrone cycloadditions (SPANC) as well as *trans*-cyclooctene-nitrone ligations that occur selectively and with high reaction velocities.^{15–23} Furthermore, nitrones provide an added level of versatility in that their reactivity can be tuned stereoelectronically, through substituent effects on both the nitrone nitrogen atom and on the adjacent carbon atoms. This tuneability has enabled duplex labelling experiments with different nitrone-alkyne pairs. However, to take full advantage of this tuneability theoretical modelling is needed.

Computational chemistry has proven to be an invaluable tool in studying bioorthogonal reaction mechanisms and allowing for multiplex labelling experiments.^{24–33} Recent work by Liang and Houk as well as others, have demonstrated that density functional theory (DFT) calculations combined with distortion/interactions (D/I) models can be useful and even predictive of

relative reactivities of different reactants in bioorthogonal reactions.³⁴ The D/I theory purports that when molecules react, they must first distort from their equilibrium geometries and that this energetic requirement is counterbalanced by a gain in energy of interactions between the distorted geometries.^{35,36} Fig. 1 shows a general example for how this would apply to SPANC reactions. When the nitrone functional group is contained within a ring, generally we have observed faster reaction kinetics that are commensurate with very high stabilities

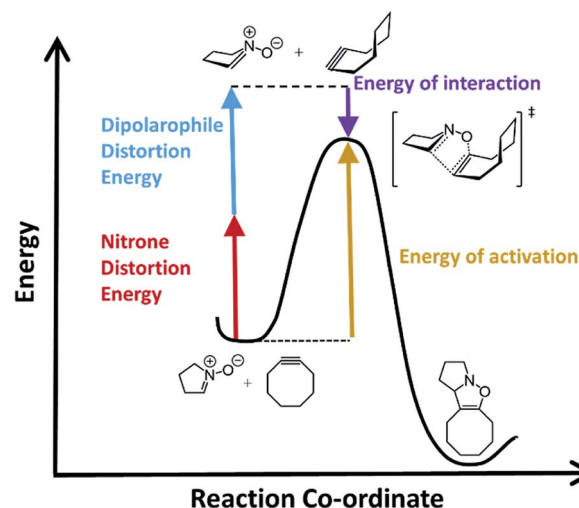


Fig. 1 An energy vs. reaction co-ordinate diagram illustrating the D/I model for bioorthogonal cycloadditions with nitrones. The red arrow represents the nitrone distortion energy, the blue arrow represents the dipolarophile distortion energy, the purple arrow represents the interaction energy, and the gold arrow represents the activation energy, respectively.

^aGraduate School of Pharmaceutical Sciences, Chiba University, 1-8-1 Inohana, Chuo-ku, Chiba, 260-8675, Japan. E-mail: m.nakajima@chiba-u.jp

^bDepartment of Chemistry and Biomolecular Sciences, University of Ottawa, 150 Louis Pasteur, Ottawa, Ontario, K1N 6N5, Canada. E-mail: john.pezacki@uottawa.ca

[†] Electronic supplementary information (ESI) available. See DOI: 10.1039/d0ra05092j



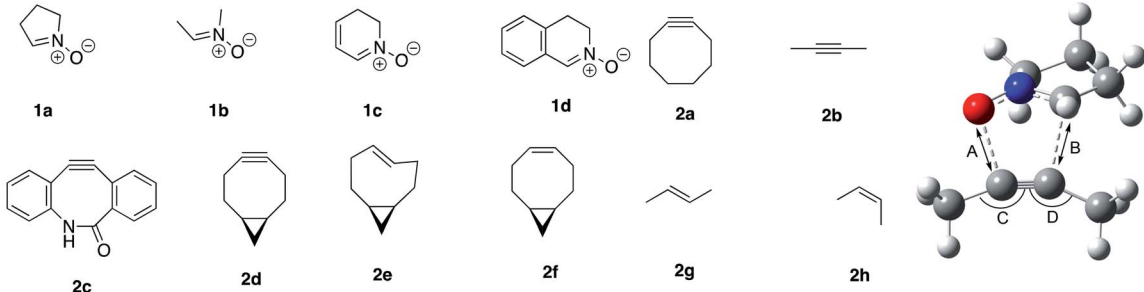
towards hydrolysis.³⁷ However, the requirement for nitron distortion is expected to be significant, thus making these reactions ideally suited for study by DFT and D/I.

In order to assess the ability of DFT and D/I to predict reactivities of nitron-based cycloaddition chemistry, we modelled 12 commonly used nitron-dipolarophile reactions using Gaussian 16, and M06-2X functionals with 6-31G* basis set.^{38–41} We also calculated the D/I energies shown in Fig. 1 for

these archetypal reactions. Single point energies were then calculated in acetonitrile (see ESI for calculated values†) and in methanol solvent (Table 1) in order to account for solvent effects on the relative energies and transitions states. The data is summarized in Table 1.

First, we used cyclooctyne **2a** for dipolarophile and compared the differences in reactivity with four kinds of nitron (Table 1 entries 1–4). The activation energy was within the range

Table 1 Calculated barriers and distortion energies for selected reactions of nitrons with dipolarophiles^a



| Entry | Nitron | Dipolarophile | k_2 (M ⁻¹ s ⁻¹) | ΔG^\ddagger (kcal mol ⁻¹) | Dis_Nitron | Dis_total | C–O distance A (Å) | CCC angle_C (°) | CCC angle_D (°) |
|-------|--------|---------------|--|---|-------------------|-----------|--------------------|------------------|------------------|
| | | | | ΔE^\ddagger (kcal mol ⁻¹) | Dis_Dipolarophile | Int | C–C distance B (Å) | Δ angle_C | Δ angle_D |
| 1 | 1a | 2a | 1.95 | 23.0 | 9.0 | 12.3 | 2.13 | 156.5 | 149.2 |
| | | | | 9.8 | 3.3 | -2.5 | 2.26 | -1.7 | -8.8 |
| 2 | 1b | 2a | N/A | 21.4 | 7.3 | 10.1 | 2.16 | 157.0 | 149.7 |
| | | | | 8.2 | 2.8 | -2.0 | 2.31 | -1.2 | -8.3 |
| 3 | 1c | 2a | N/A | 21.6 | 7.9 | 11.0 | 2.12 | 155.8 | 150.3 |
| | | | | 8.6 | 3.1 | -2.3 | 2.29 | -2.4 | -7.7 |
| 4 | 1d | 2a | 1.5 | 21.8 | 8.1 | 11.3 | 2.10 | 155.6 | 149.9 |
| | | | | 8.4 | 3.3 | -2.9 | 2.31 | -2.6 | -8.1 |
| 5 | 1a | 2b | N/A | 35.4 | 12.3 | 24.4 | 2.08 | 161.1 | 153.4 |
| | | | | 20.5 | 12.1 | -3.9 | 2.21 | -18.8 | -26.6 |
| 6 | 1a | 2c | 41.7 | 13.0 | 3.4 | 4.8 | 2.20 | 150.5 | 142.4 |
| | | | | -1.2 | 1.4 | -6.0 | 2.46 | -5.3 | -9.5 |
| 7 | 1a | 2c | 39.9 | 12.9 | 4.4 | 5.8 | 2.24 | 145.8 | 143.1 |
| | | | | -0.7 | 1.4 | -6.5 | 2.41 | -12.7 | -8.8 |
| 8 | 1a | 2d | 0.05 | 20.6 | 6.8 | 9.1 | 2.17 | 154.5 | 147.0 |
| | | | | 7.3 | 2.3 | -1.8 | 2.33 | -0.3 | -7.7 |
| 9 | 1a | 2d | 0.05 | 20.8 | 6.9 | 9.3 | 2.16 | 154.4 | 146.8 |
| | | | | 7.5 | 2.4 | -1.8 | 2.34 | -0.4 | -7.9 |
| 10 | 1a | 2e | 0.08 | 21.9 | 7.4 | 9.9 | 2.15 | | |
| | | | | 8.1 | 2.6 | -1.8 | 2.37 | | |
| 11 | 1a | 2e | 0.08 | 22.0 | 7.6 | 10.2 | 2.17 | | |
| | | | | 8.3 | 2.6 | -1.9 | 2.35 | | |
| 12 | 1a | 2f | N/A | 28.9 | 12.8 | 18.9 | 2.11 | | |
| | | | | 14.4 | 6.0 | -4.4 | 2.20 | | |
| 13 | 1a | 2f | N/A | 32.6 | 14.4 | 23.3 | 2.10 | | |
| | | | | 18.0 | 9.0 | -5.4 | 2.18 | | |
| 14 | 1a | 2g | N/A | 32.0 | 14.5 | 24.2 | 2.08 | | |
| | | | | 18.2 | 9.7 | -6.0 | 2.20 | | |
| 15 | 1a | 2h | N/A | 30.6 | 13.2 | 21.0 | 2.11 | | |
| | | | | 16.1 | 7.8 | -4.9 | 2.18 | | |

^a Geometry optimizations were carried out at the M06-2X level of theory with the 6-31G(d) basis set. Solvent effects in methanol were evaluated at the M06-2X/6-311++G(d,p) level at 298.15 K with a self-consistent reaction field (SCRF) using the SMD model on the gas-phase-optimized structures. Dis_nitron is the distortion energy for the nitrons shown, dis_dipolarophile is the distortion energy for the different dipolarophiles shown, dis_total refers to the total distortion energy, and int represents the interaction energy for the given reaction. The C–O and C–C bond distances are for the bond lengths at the transition states for the bonds forming in the reactions. The bond angles represent those in the illustration above the table. Rate constants were measured previously.^{17,23,42,43}



of 21.4–23.0 kcal mol^{−1}, and **1b** gave the smallest value. Distortion energy of nitrones also had the smallest value for **1b**, suggesting that **1b** had the least steric hindrance (entry 2). In addition, **1a**, which contains a relatively large amount of sp³ carbons, has the highest distortion energy, and **1d**, which includes a relatively large amount of sp² carbons and conjugated aromatic ring, has the highest interaction energy (entries 1 and 4).

Next, using **1a** for the nitrone reactant, we compared four alkynes (Table 1, entries 1, 5–9). We determined that the maximum activation energy of 35.4 kcal mol^{−1} was obtained in 2-butyne (**2b**), for which the structure is not distorted and is linear (entry 5). It can be seen that the distortion energy of dipolarophile is as large as 12.1 kcal mol^{−1}; the Me-CC bond angle of alkyne in the transition state is distorted by −18.9° and −26.7°, respectively. In addition, because the atomic distance of the newly formed C–C and C–O bond in the transition state is shorter, deformation also occurs in the nitrone, and the value of distortion energy becomes large. Thus, according to Hammond postulate, the reaction of unstrained **2b** has a late transition state and shows large activation energy.

The benzannulated cyclooctyne **2c** showed the smallest activation energy (entries 6 and 7). Interestingly, in both regioisomers, the distortion of the bond angles of the alkyne in the transition state are −5.4° and −9.5°, or −12.8° and 8.8°, respectively, which is larger than that of cyclooctyne **2a** (entry 1). However, the distortion energies of **2c** in the transition state are 1.60 and 1.89 kcal mol^{−1}, which are the smallest of all. Therefore, for **2c**, it was revealed that the distortion of the CCC bond angle had no significant effect on the energy change at the transition state.

For bicyclononyne **2d**, both diastereomers gave similar results (entries 8 and 9). Distortion energies of both nitrone and dipolarophile were smaller than that of cyclooctyne, probably because of the conformational restriction introduced by the fused cyclopropane ring. Finally, the calculation was performed using cycloalkenes as well as linear alkenes and a linear alkyne as dipolarophiles (entries 10–15). The results showed that in the strained *trans*-cyclooctene (TCO), the activation barrier and distortion energy were smaller than that of the cyclooctyne, indicating that the reaction proceeds by early transition state. On the other hand, unstrained olefins, *cis*-cyclooctene and *trans/cis*-butene, show large activation energy and distortion energy, implying the late transition states and energetically unfavourable reactions relative to the other dipolarophiles studied.

As had been observed previously, we also found that the relative contribution of alkyne or alkene distortion energy was directly proportional to the spontaneity of the reactions.⁴² In Fig. 2A, we plotted the bond length of the newly forming C–C and C–O bonds in the transition states for the cycloaddition reactions against the nitrone distortion energies. We observed that the nitrone distortion energies increase as the transition state position moves towards the products of the reaction. The longer bond lengths represent earlier transition states according to the Hammond postulate.

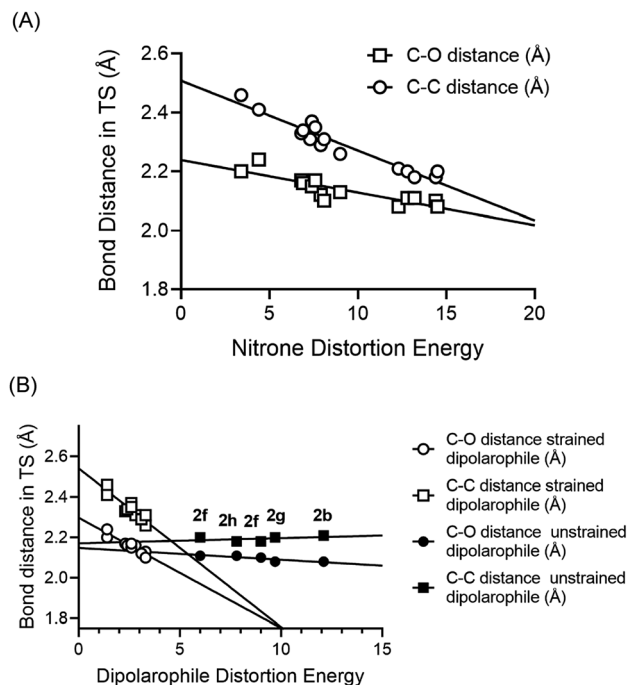


Fig. 2 (A) Plots of C–C and C–O bond distances in the computed transition states vs. the distortion energy of the nitrones from the different entries from Table 1. (B) Plots of C–C and C–O bond distances in the computed transition states vs. the distortion energy of the dipolarophiles from the different entries from Table 1. In this case two different trend lines were observed, a relatively flat trendline for the unstrained alkenes and alkynes and a steeper dependency for the strained cyclooctynes and TCO.

For the distortion energies of the dipolarophiles, two distinct trends were observed. In Fig. 2B we plotted the bond length of the newly forming C–C and C–O bonds in the transition states for the cycloaddition reactions against the dipolarophile distortion energies. Here we observed that unstrained dipolarophiles **2b**, **2f–h** all displayed differences in distortion energies that were not dependent on the position of the transition state. However, the strained cyclooctynes and TCO both displayed strong correlation between distortion energies and the position of the transition state.

For SPANC reactions we clearly observe an important dependence on overall barrier for reactions towards both distortion energies of alkyne and nitrone. For cyclooctynes that are already more strained and distorted in the ground state, these effects are magnified, as is the case for entries 6 and 7, and to a lesser extent entry 8 as compared with entries 1–4.

Recently we have reported that nitrones will react with different *trans*-cyclooctenes (TCO) in TCO–nitrone ligation reactions.²³ While these reactions are somewhat slower than their tetrazine counterparts, they still represent useful chemical transformations with utility in bioorthogonal applications and give other applications to TCOs when tetrazine reactions are not possible. Here our analyses show that strained TCO (s-TCO) has little requirement for distortion prior to reaching the transition state with nitrone reaction partners and that nitrone reaction partners also do not need to achieve significant distortion in the



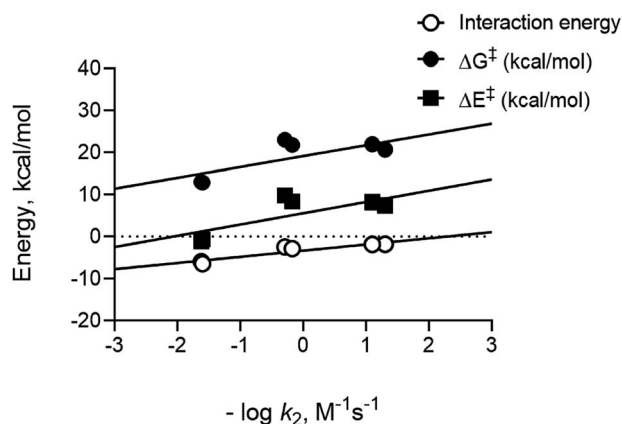


Fig. 3 Plots of computed parameters versus the negative log of the bimolecular rate constants for the analogous reactions determined experimentally. The data establish linear free energy relationships between computed and experimental data and showing proportionality between the experimental energies of activation at room temperature.

transition state, Table 1, entries 10 and 11 as compared with entries 12–15. The relative contributions are comparable with the reactions of the same nitron with bicyclononyne (BCN). When comparing results for *cis*-cyclooctene and acyclic alkenes and their reactions with nitrones, both barriers for reactions and distortion energies increase dramatically, as expected. Generally speaking, *cis*-alkenes should be slightly more reactive in reactions with dipoles, with exception to s-TCO where strain energy and distortion greatly outweigh steric approach control. Again, DFT and D/I provide a useful framework for predicting the reactions of different nitrones with TCOs.

To compare calculated energies with experimental data, we used rate constant data previously measured for entries where numbers were available.^{17,23,42,43} Since rate constants are related to reaction barriers through transition state theory, we plotted the negative log of the bimolecular rate constants versus calculated parameters. Importantly, distortion energies calculated for nitrones and dipolarophiles do not readily predict the trend in reactivities that we observe experimentally. Rather, we only see the interaction energies for the different reactions follow a linear trend demonstrating a linear free energy relationship between these computed energies and experimental data, see Fig. 3. Good correlation for interactions energies suggest that they play an important role in defining the relative barrier heights for the reaction. The overall observed correlation suggests that the D/I model accurately predicts the relative reactivities for nitron cycloadditions in solution, thus confirming the applicability of D/I theory with respect to predicting reactivity trends for both SPANC and TCO–nitron ligation reactions.

Conclusions

We have examined the reactivities of some common and useful nitron cycloadditions using density functional theory (DFT) and applied the distortion/interaction model. Our results show

that these methods predict relative reactivities as compared with experimental results. Nitron distortion energies appear to follow a trend that reflects their relative contribution to the overall transition state structure. Interestingly, the total interaction energies for the different reactions modeled to play a dominant role in affecting relative barrier heights for reactions involving both strained alkynes and *trans*-cyclooctenes. The relative magnitudes of the interaction energies appear to predict the relative reactivity and trends in reactivities. In summary, we have found that D/I theory can explain experimental trends in reactivity for cycloadditions involving nitrones and provide a convenient tool to predict reactivity that is useful in planning and experimental design. Future studies will focus on computations involving other nitron cycloaddition reactions, as well as studying the potential for other mutually orthogonal reactions for multiplex labelling experiments.

Conflicts of interest

There are no conflicts to declare.

Acknowledgements

We thank Natural Sciences and Engineering Council of Canada (NSERC) for financial support for this project, in the form of a discovery grant to J.P. Pezacki. Numerical calculations were carried out on the SR24000 computer at the Institute of Management and Information Technologies, Chiba University.

Notes and references

- 1 D. M. Patterson, L. A. Nazarova and J. A. Prescher, *ACS Chem. Biol.*, 2014, **9**, 592–605.
- 2 E. M. Sletten and C. R. Bertozzi, *Angew. Chem., Int. Ed.*, 2009, **48**, 6974–6998.
- 3 C. S. McKay and M. G. Finn, *Chem. Biol.*, 2014, **21**, 1075–1101.
- 4 A. F. L. Schneider and C. P. R. Hackenberger, *Curr. Opin. Biotechnol.*, 2017, **48**, 61–68.
- 5 G. Liu, E. A. Wold and J. Zhou, *Curr. Top. Med. Chem.*, 2019, **19**, 892–897.
- 6 A. Godinat, A. A. Bazhin and E. A. Goun, *Drug Discovery Today*, 2018, **23**, 1584–1590.
- 7 E. M. Sletten and C. R. Bertozzi, *Acc. Chem. Res.*, 2011, **44**, 666–676.
- 8 A. Vázquez, R. Dzajak, M. Dračinský, R. Rampmaier, S. J. Siegl and M. Vrabec, *Angew. Chem., Int. Ed.*, 2017, **56**, 1334–1337.
- 9 B. Akgun, C. Li, Y. Hao, G. Lambkin, R. Derda and D. G. Hall, *J. Am. Chem. Soc.*, 2017, **139**, 14285–14291.
- 10 A. Mamot, P. J. Sikorski, M. Warminski, J. Kowalska and J. Jemielity, *Angew. Chem., Int. Ed.*, 2017, **129**, 15834–15838.
- 11 C. P. Ramil, M. Dong, P. An, T. M. Lewandowski, Z. Yu, L. J. Miller and Q. Lin, *J. Am. Chem. Soc.*, 2017, **139**, 13376–13386.
- 12 T. S. Tang, H. Liu and K. K. Lo, *Chem. - Eur. J.*, 2016, **22**, 9649–9659.
- 13 R. D. Row and J. A. Prescher, *Acc. Chem. Res.*, 2018, **51**, 1073–1081.



- 14 S. Ghiassian, L. Yu, P. Gobbo, A. Nazemi, T. Romagnoli, W. Luo, L. G. Luyt and M. S. Workentin, *ACS Omega*, 2019, **4**, 19106–19115.
- 15 D. A. Mackenzie, A. R. Sherratt, M. Chigrinova, L. L. W. Cheung and J. P. Pezacki, *Curr. Opin. Chem. Biol.*, 2014, **21**, 81–88.
- 16 D. A. Mackenzie and J. P. Pezacki, *Can. J. Chem.*, 2014, **92**, 337–340.
- 17 C. S. McKay, J. A. Blake, J. Cheng, C. Danielson and J. P. Pezacki, *Chem. Commun.*, 2011, **47**, 10040–10042.
- 18 A. R. Sherratt, M. Chigrinova, D. A. Mackenzie, N. K. Rastogi, M. T. M. Ouattara, A. T. Pezacki and J. P. Pezacki, *Bioconjugate Chem.*, 2016, **27**, 1222–1226.
- 19 D. A. Mackenzie, A. R. Sherratt, M. Chigrinova, A. J. Kell and J. P. Pezacki, *Chem. Commun.*, 2015, **51**, 12501–12504.
- 20 M. Colombo, S. Sommaruga, S. Mazzucchelli, L. Polito, P. Verderio, P. Galeffi, F. Corsi, P. Tortora and D. Prosperi, *Angew. Chem., Int. Ed.*, 2012, **51**, 496–499.
- 21 P. N. Gunawardene, W. Luo, A. M. Polgar, J. F. Corrigan and M. S. Workentin, *Org. Lett.*, 2019, **21**, 5547–5551.
- 22 W. Luo, J. Luo, V. V. Popik and M. S. Workentin, *Bioconjugate Chem.*, 2019, **30**, 1140–1149.
- 23 K. D. Margison, D. A. Bilodeau, F. Mahmoudi and J. P. Pezacki, *ChemBioChem*, 2020, **21**, 948–951.
- 24 Y. Liang, J. L. MacKey, S. A. Lopez, F. Liu and K. N. Houk, *J. Am. Chem. Soc.*, 2012, **134**, 17904–17907.
- 25 C. G. Gordon, J. L. MacKey, J. C. Jewett, E. M. Sletten, K. N. Houk and C. R. Bertozzi, *J. Am. Chem. Soc.*, 2012, **134**, 9199–9208.
- 26 P. An, T. M. Lewandowski, T. G. Erbay, P. Liu and Q. Lin, *J. Am. Chem. Soc.*, 2018, **140**, 4860–4868.
- 27 D. N. Kamber, Y. Liang, R. J. Blizzard, F. Liu, R. A. Mehl, K. N. Houk and J. A. Prescher, *J. Am. Chem. Soc.*, 2015, **137**, 8388–8391.
- 28 M. K. Narayanam, Y. Liang, K. N. Houk and J. M. Murphy, *Chem. Sci.*, 2016, **7**, 1257–1261.
- 29 Y. Fang, H. Zhang, Z. Huang, S. L. Scinto, J. C. Yang, C. W. Am Ende, O. Dmitrenko, D. S. Johnson and J. M. Fox, *Chem. Sci.*, 2018, **9**, 1953–1963.
- 30 W. D. Lambert, S. L. Scinto, O. Dmitrenko, S. J. Boyd, R. Magboo, R. A. Mehl, J. W. Chin, J. M. Fox and S. Wallace, *Org. Biomol. Chem.*, 2017, **15**, 6640–6644.
- 31 H. Tao, F. Liu, R. Zeng, Z. Shao, L. Zou, Y. Cao, J. M. Murphy, K. N. Houk and Y. Liang, *Chem. Commun.*, 2018, **54**, 5082–5085.
- 32 T. Bettens, M. Alonso, P. Geerlings and F. De Proft, *Chem. Sci.*, 2020, **11**, 1431–1439.
- 33 J. G. de la Concepción, M. Ávalos, P. Cintas and J. L. Jiménez, *Chem. - Eur. J.*, 2018, **24**, 7507–7512.
- 34 F. Liu, Y. Liang and K. N. Houk, *Acc. Chem. Res.*, 2017, **50**, 2297–2308.
- 35 D. H. Ess and K. N. Houk, *J. Am. Chem. Soc.*, 2008, **130**, 10187–10198.
- 36 D. H. Ess and K. N. Houk, *J. Am. Chem. Soc.*, 2007, **129**, 10646–10647.
- 37 C. S. McKay, J. A. Blake, J. Cheng, D. C. Danielson and J. P. Pezacki, *Chem. Commun.*, 2011, **47**, 10040–10042.
- 38 R. A. Miranda-Quintana, M. M. González, D. Hernández-Castillo, L. A. Montero-Cabrera, P. W. Ayers and C. Morell, *J. Mol. Model.*, 2017, **23**, 1–15.
- 39 A. I. Adjieufack, I. M. Ndassa, J. K. Mbadcam, M. Ríos-Gutiérrez and L. R. Domingo, *Theor. Chem. Acc.*, 2017, **136**, 1–12.
- 40 R. Herrera, A. Nagarajan, M. A. Morales, F. Méndez, H. A. Jiménez-Vázquez, L. G. Zepeda, J. Tamariz and J. Tamariz, *J. Org. Chem.*, 2001, **66**, 1252–1263.
- 41 E. A. Bofo, K. Darko, B. A. Afriyie, R. Tia and E. Adei, *J. Mol. Graphics Modell.*, 2018, **81**, 1–13.
- 42 C. S. McKay, M. Chigrinova, J. A. Blake and J. P. Pezacki, *Org. Biomol. Chem.*, 2012, **10**, 3066–3070.
- 43 C. S. McKay, J. Moran and J. P. Pezacki, *Chem. Commun.*, 2010, **46**, 931–933.

